Here, we study the influence of the curvature-induced DMI on the magnetic vortex state in spherical caps made of an intrinsically achiral and isotropic ferromagnet. Similarly to spherical shells [40], the effective DMI in a spherical cap leads to the additional tilt of the azimuthal angle of magnetization. The presence of an edge for the spherical cap allows non-zero tilt angle of magnetization at the edge. Furthermore, we show that the effective DMI in spherical caps increases the size of the magnetic vortex core for any combination of vortex polarity and circulation. This effect is different compared to the case of a planar disk, where the intrinsic DMI can either decrease or increase the vortex core size dependent on the sign of the product of circulation and polarity with respect to the sign of the DMI constant [50].

2. Model of a spherical cap

The first theory of curvilinear magnetism was formulated by Gaididei *et al*. [42] to describe local effects in curved magnetic shells. A unified description of the curvature-induced effects is based on a micromagnetic framework of curvilinear magnetism [44], which allows considering local and nonlocal interactions on equal footing. In this work, we will discuss magnetic properties of ultrathin ferromagnetic shells of magnetically soft material, taking into account exchange and magnetostatic interactions only: $E = \int \mathrm{d}\mathbf{r}\left(\mathcal{E}^{\mathrm{x}} + \mathcal{E}^{\mathrm{ms}}\right)$. The energy density of the isotropic exchange interaction is written as $\mathcal{E}^{\mathrm{x}} = -A\mathbf{m}\cdot\nabla^2\mathbf{m}$, with $\mathbf{m}$ being the normalized magnetization and A being the exchange constant. It is established that not only for the case of ultrathin planar films [51–54] but also for ultrathin geometrically curved shells the magnetostatic energy $\mathcal{E}^{\mathrm{ms}}$ can be reduced to the shape-induced easy-surface anisotropy $\mathcal{E}_{\mathrm{A}}^{\mathrm{ms}}$ [55, 56]. In our model, the sample geometry enters the description only through the anisotropy term $\mathcal{E}_{\mathrm{A}}^{\mathrm{ms}} = K\left(\mathbf{m}\cdot\hat{\mathbf{n}}\right)^2$, where the effective anisotropy constant $K = 2\pi M_s^2$ with M_s being the saturation magnetization. Here, a coordinate-dependent unit normal vector $\hat{\mathbf{n}} = \hat{\mathbf{n}}(\mathbf{r})$ determines the direction of the magnetic hard axis.

The current micromagnetic approach requires that the sample has a constant thickness h along the normal. This makes it possible to suppose that the magnetization does not depend on the normal coordinate. This assumption is valid in the limit of ultrathin shells, namely the shell thickness h should be much smaller than the typical magnetic length scale $\ell = \sqrt{A/K}$. One more restriction is that h should be much smaller than the typical curvature radii L. Then, one can systematize geometrical effects by restructuring all magnetic energy terms according to their local spatial symmetry:

$$E = Ah\int_S dS\left(\mathcal{E}_0 + \mathcal{E}_{\mathrm{A}} + \mathcal{E}_{\mathrm{D}}\right). \tag{1}$$

The first energy density contribution $\mathcal{E}_0 = \eth_\alpha m_i \eth_\alpha m_i$ is a regular isotropic part of the exchange energy, it is similar to the one in a planar film. Here m_i is an ith magnetization component in the curvilinear orthonormal Darboux three-frame $\{\mathbf{e}_1, \mathbf{e}_2, \hat{\mathbf{n}}\}$ on the surface, where $\mathbf{e}_1$ and $\mathbf{e}_2$ are unit vectors corresponding to the principal directions. Here and below we use Greek letters α, β, γ run values 1, 2 and refer to the curvilinear coordinates on the surface; to indicate all three components of any vector, we use Latin indices $i, j = 1, 2, n$. The Einstein summation convention is also assumed. The notation $\eth_\alpha$ is used for tangential derivatives,

$$\eth_\alpha m_\beta = \left(\mathfrak{g}_{\alpha\alpha}\right)^{-1/2}\left[\partial_\alpha m_\beta + \varepsilon_{\beta\gamma}\left(\mathbf{e}_1\cdot\partial_\alpha\mathbf{e}_2\right)m_\gamma\right] \text{ and}$$

$$\eth_\alpha m_n = \left(\mathfrak{g}_{\alpha\alpha}\right)^{-1/2}\partial_\alpha m_n$$

with $\mathfrak{g}_{\alpha\beta}$ being the metric tensor and $\varepsilon_{\beta\gamma}$ being totally antisymmetric tensor [44].

The second term, an effective anisotropy, $\mathcal{E}_{\mathrm{A}}$ comprises the shape-induced anisotropy $\mathcal{E}_{\mathrm{A}}^{\mathrm{ms}}$ and the curvature-induced exchange-driven biaxial anisotropy $K_{ij}m_i m_j$, where K_{ij} have a bilinear form with respect to the principle curvatures κ_1 and κ_2 of the surface, $K_{ij} = A\kappa_i^2\delta_{ij}$ with $\kappa_n^2 \equiv \kappa_1^2 + \kappa_2^2$. The curvature-induced exchange-driven DMI $\mathcal{E}_{\mathrm{D}} = D_\alpha \mathcal{L}_{\alpha n}^{(\alpha)}$ is determined by the curvilinear analog of Lifshitz invariants $\mathcal{L}_{ij}^{(\alpha)} = m_i\eth_\alpha m_j - m_j\eth_\alpha m_i$ [44]. It is worth noting that in the general case of an arbitrary surface, the intensity of the curvature-induced DMI depends on two principal curvatures $D_\alpha = 2A\kappa_\alpha$.

In the current study, we limit our consideration to a spherical cap structure with the inner radius L, the cut angle ϑ_0 and thickness $h \ll \ell \ll L$, see Fig. 1. In the case of a spherical surface, both principal curvatures read $\kappa_{1,2} = 1/L$.

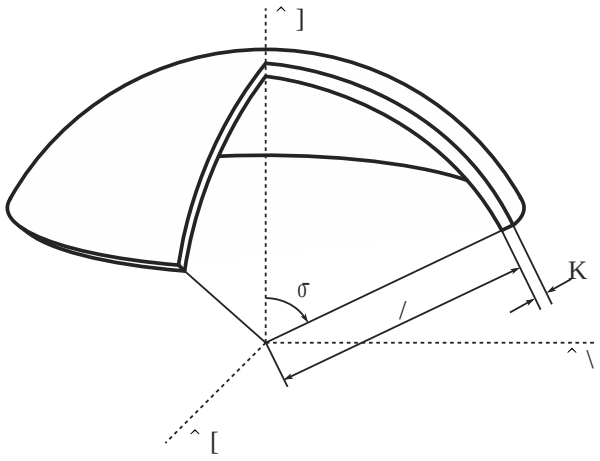

Fig. 1. Schematic of a spherical cap. The cap is formed by two spherical surfaces with the inner sphere having radius L. The thickness of the cap is h. The edge surface of the cap is formed by the intersection of the two spherical surfaces by a cone with the opening angle ϑ_0.

Then the effective anisotropy $\mathcal{E}_A = K_{ef}\left(\mathbf{m}\cdot\hat{\mathbf{n}}\right)^2$ with the effective anisotropy constant $K_{ef} = A/\ell^2 + A/L^2$. Both curvature-induced DMI coefficients are equal and inversely proportional to the curvature radius $D_\alpha = 2A/L$.

The ground state of a spherical cap is known to depend on the material and geometrical parameters of the sample [15, 57]. In particular, while the vortex state is observed for caps of large diameters, the onion state is realized for thin caps of small diameter, and a uniform easy-axis state is favorable for caps of small diameter and large thickness.

3. In-surface magnetization curling

It was predicted by Butenko *et al.* [50, 58] and experimentally confirmed by Im *et al.* [59], that intrinsic DMI leads to significant changes of the magnetic vortex texture in planar disks. Namely, the intrinsic DMI of surface type favors the magnetization curling with the rotation direction being determined by the sign of the Dzyaloshinskii constant, resulting in the increase or decrease of the vortex core size depending on the vortex chirality. In the following, we discuss the influence of the curvature-induced DMI on the properties of the magnetic vortex in a cap and compare the predicted effects to those induced by the intrinsic DMI.

It is instructive to start the analysis for spherical shells whose size allows supporting strongly inhomogeneous magnetic textures instead of spontaneous formation of ferromagnetic domains [21]. For the case of a Heisenberg easy-surface ferromagnet shaped in spherical shell geometry, the vortex state is realized only with the same polarity on both poles (the vortex polarity is defined with respect to the surface normal). A symmetry of the magnetic texture forces the equatorial magnetization to be strictly parallel to the equator of the sphere [40]. This symmetry is absent for the case of a magnetically soft spherical cap, which can host the only one vortex. Therefore, it is to be expected that the edge magnetization **m** experiences tilt by an angle $\psi(\vartheta_0)$, which is dependent on the opening angle ϑ_0 of the cap, see Fig. 1. To determine this tilt, we carried out series of micromagnetic simulations using magpar code [60, 61]. Technically, we performed energy minimization for spherical caps with the inner radius $L = 50$ nm and shell thickness $h = 5$ nm for different opening angles ϑ_0. For simulations, material parameters similar to Permalloy (Py, $Ni_{81}Fe_{19}$) were used: exchange constant $A = 10.5$ pJ/m and saturation magnetization $M_s = 795$ kA/m. These parameters result in the exchange length $\ell \approx 5.14$ nm. We utilize the spherical angle parametrization for the spherical curvilinear coordinates (ϑ, χ, r) of the magnetization unit vector **m**, namely, $m_1 \equiv m_\vartheta = \sin\theta\cos\phi$, $m_2 \equiv m_\chi = \sin\theta\sin\phi$, and $m_n \equiv m_r = \cos\theta$. For the vortex distribution in a thin spherical cap

$$\theta = \theta(\vartheta), \quad \phi = \mathfrak{C}\left(\frac{\pi}{2} + \psi\right),$$

where $\psi = \psi(\vartheta)$ represents the tilt angle and $\mathfrak{C} = \pm 1$ determines the vortex circulation. Figure 2 summarizes the results of micromagnetic simulations on the determination of the magnetization tilt at the edge of the cap for different opening angles ϑ_0. The tilt angle ψ has not zero value near the cap edge and increases in the vicinity of the vortex core. At the same time, an increase of the cap opening angle ϑ_0 does not lead to significant changes of the tilt angle ψ near the vortex core. On the other hand, increasing the opening angle results in the decrease of the tilt angle at the edge, see inset in Fig. 2. This effect can be explained by the increase of the distance between the vortex core and cap edge with the increase of the opening angle.

To describe the tilt angle in a spherical cap theoretically, it is convenient to use the following notation, which corresponds to the stereographic projection on a plane:

$$\rho = \frac{1}{R}\tan\frac{\vartheta}{2}, \qquad \rho \in [0,1), \qquad R = \frac{1}{L}\tan\frac{\vartheta_0}{2}. \tag{2}$$

Using this notation, one can write the Euler–Lagrange equations for the spherical geometry [40] in the following form:

$$\theta'' + \frac{\theta'}{\rho} + \sin\theta\cos\theta\left(\mathcal{K} - \frac{1}{\rho^2}\right) - \mathcal{D}\frac{\sin^2\theta}{\rho} = 0, \tag{3a}$$

$$\psi'' + \frac{\psi'}{\rho} + 2\cot\theta\theta'\psi' + 2\cos\psi\frac{2R}{1+R^2\rho^2}\theta' = 0, \tag{3b}$$

where prime symbols correspond to the derivative with respect to ρ. Effective anisotropy $\mathcal{K}$ and effective DMI $\mathcal{D}$ are functions of the coordinate ρ:

$$\begin{aligned} \mathcal{K}(\rho) &= \frac{R^2}{\beta^2(1+R^2\rho^2)^2} - (\psi')^2, \quad \beta = \frac{\ell}{2\sqrt{L^2+2\ell^2}}, \\ \mathcal{D}(\rho) &= 4\left(\frac{\rho R}{1+\rho^2R^2}\sin\psi\right)', \end{aligned} \tag{4}$$

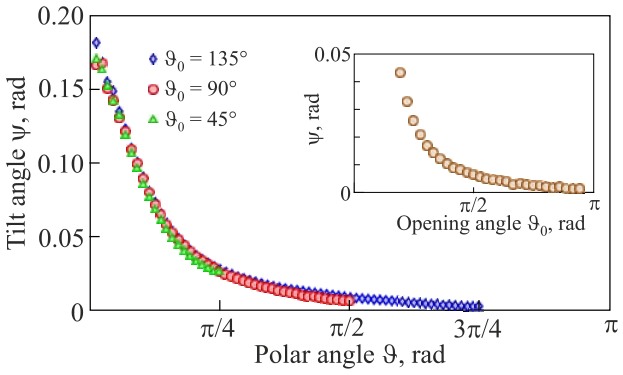

Fig. 2. (Color online) Dependence of the tilt angle ψ on the polar angle ϑ for a spherical cap with inner radius $L = 50$ nm, thickness $h = 5$ nm and different opening angles ϑ_0. Inset shows how the tilt ψ at the cap edge depends on cap opening angle ϑ_0. The plots are obtained from micromagnetic simulations.

One has to stress that the stereographic projection (2) is a particular mapping that projects a sphere onto a plane. Nevertheless, it is the only mapping that allows to reconstruct the planar skyrmion equation; for generalization of the mapping (2) for arbitrary surface of revolution, see [49]. In the case $\mathcal{K}$ = const and $\mathcal{D}$ = const, equation (3a) resembles a typical vortex-like equation for easy-plane film with DMI [50, 58]. For the case of a curvilinear shell, the stereographic projection introduces a nonlinear coordinate dependency even for spherical surfaces with a constant curvature. An effective coordinate-dependent anisotropy $\mathcal{K}$ and DMI $\mathcal{D}$ was discussed in details for skyrmionium states engineered by the gradient of the curvature [49].

The key novelty of this manuscript is in the coupling of Eq. (3b) with Eq. (3a) by effective anisotropy and DMI. It is important to mention that the coordinate dependence of the effective DMI constant $\mathcal{D}$ does not lead to the driving on magnetic solitons. This is in contrast to the case of the skyrmion equation in curvilinear shells of more complex geometry [48, 49]. The difference is due to the constant curvature of the geometry (spherical shell).

The curvature-induced DMI and anisotropy depend on the reduced polar angle ρ. In the limiting case of a disk ($\vartheta_0 \to 0$ keeping the product $\vartheta_0 L$ = const) the solution of the second equation in Eq. (3) is $\psi = 0$ (tilt angle disappears for planar disks). Consequently, $\mathcal{D} = 0$, which means that the curvature-induced DMI disappears for planar disks.

The equations (3) can be solved numerically with the boundary condition $\theta(0) = 0$, $\theta(1) = \pi/2$, $\psi'(0) = 0$, and $\psi(1) + d\psi'(1) = 0$, where d describes a pinning effect introduced by the surface energy at the cap edge. The parameter d can be found from micromagnetic simulations. For Py spherical cap with inner radius $L = 50$ nm, thickness $h = 5$ nm, and opening angle $\vartheta_0 = \pi/2$, the pinning parameter $d \approx 0.47$. The numerical solution of Eq. (3) is shown in Fig. 3 (red line in the main figure and black line in the inset). The obtained out-of-surface component $\theta(\rho)$ is in good agreement with the result of full scale micromagnetic simulations (red symbols). On the other hand, the numerical solution for the tilt angle ψ differs significantly from the full scale micromagnetics. This can be explained by the fact that Eq. (3) are written for the Heisenberg easy-surface ferromagnet without nonlocal magnetostatic effects. In contrast, the full scale magnetostatic simulations account for not only surface but also volume charges that increase the total energy. To verify this assumption, we performed additional simulations of a Heisenberg easy-surface ferromagnet shaped as a spherical cap with the following parameters: exchange constant $A = 10.5$ pJ/m and anisotropy constant $K = 398$ kJ/m^3. These parameters result in the magnetic length $\ell \approx 5.14$ nm (the same value as for the exchange length above). The tilt angle ψ obtained from simulations of this model is displayed in Fig. 3 by blue diamonds, which fits the numerical solution of Eq. (3) well. We observe that volume charges

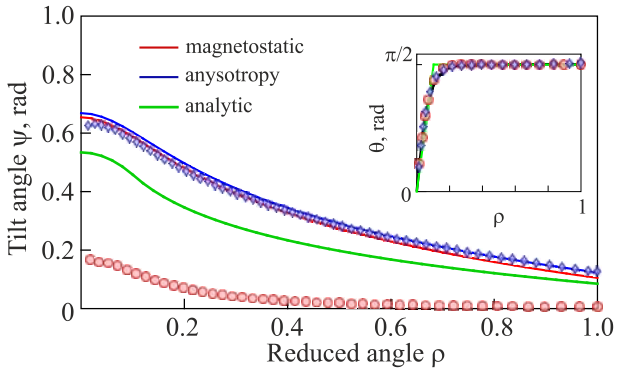

Fig. 3. (Color online) Magnetic vortex parameters vs reduced angle ρ. Comparison of the results of micromagnetic simulations (symbols) with the analytic and numerical solution (solid lines) of the Euler–Lagrange equations (3). Red circles correspond to the simulation results for the model with full scale magnetostatics. Blue diamonds correspond to the simulation results for the model with easy-surface anisotropy. Red and blue solid lines correspond to the numerical solution of Eq. (3) with the pinning parameter $d = 0.47$ (model with full scale magnetostatics) and $d = 0.52$ (model with easy-surface anisotropy), respectively. Green line corresponds to the analytic solution (6). Inset shows the out-of-surface component of magnetization θ for each of these models. The shown dependences are calculated for the Permalloy spherical cap with inner radius $L = 50$ nm, thickness $h = 5$ nm and opening angle $\vartheta_0 = \pi/2$.

that are not taken into account in the later simulations of a cap with the easy-surface anisotropy lead to the decrease of the tilt angle ψ, while vortex core profile remains the same (blue diamonds in the inset of Fig. 3). Simulations of the model with the effective easy-surface anisotropy allow estimating the pinning parameter $d = 0.52$.

To analyze the tilt angle analytically, we use the following model for the angular parameter of the out-of-surface component of the magnetic vortex texture:

$$\theta = \begin{cases} \dfrac{\pi}{2} p\left(\dfrac{\rho}{\rho_c} - 1\right) + \dfrac{\pi}{2}, & \rho < \rho_c \\ \dfrac{\pi}{2}, & \rho \geq \rho_c, \end{cases} \tag{5}$$

where p determines the vortex polarity and ρ_c determines the size of the vortex core. In the case of a planar nanomagnet, the size of the vortex core can be determined as 2ℓ. Consequently, for a spherical cap, we can expect $\rho_c \approx \tan(\ell / L)$. Substituting Eq. (5) into (3b), we find the solution for the case $\rho_c \ll 1$:

$$\psi = \begin{cases} \psi^{<} = \phi_1 - \phi_0 \rho^2, & \rho < \rho_c, \\ \psi^{>} = \phi_2 \ln \rho + \phi_3, & \rho \geq \rho_c, \end{cases} \tag{6}$$

where ϕ_0 can be found from Eq. (4) and constants ϕ_1, ϕ_2, ϕ_3 can be found from the condition

$$\left[\frac{\psi'}{\psi}\right]_{\rho_c} = 0, \quad \psi(1) + d\psi'(1) = 0.$$

Finally, constants in Eq. (6) read:

$$\phi_0 = \frac{\pi}{4}\frac{1}{\rho_c} pR, \quad \phi_1 = \frac{\pi}{4} pR\rho_c \left(1 + 2d - 2\ln\rho_c\right), \\ \phi_2 = -\frac{\pi}{2} pR\rho_c, \quad \phi_3 = \frac{\pi}{2} pR\rho_c d. \tag{7}$$

The analytical solution, Eq. (6) (green line in Fig. 3), slightly underestimates the tilt angle ψ compared to the numerical solution of Eq. (3) (blue line in Fig. 3) and simulation results (blue diamonds in Fig. 3) for the model with easy-surface anisotropy. The observed discrepancy is due to a rather crude model used for the description of the out-of-surface angular component of magnetization.

4. Out-of-surface component of magnetization

Butenko *et al*. analyzed the impact of the intrinsic DMI of volume type on vortices in planar disks [50]. The Euler–Lagrange equation for the out-of-surface magnetization obtained for the case of planar disks with the volume type DMI [50] has the same form as the Euler–Lagrange equation (3) for θ for the case of spherical caps. Thus, it is insightful to compare the influence of the curvature-induced DMI on the out-of-surface magnetization component of vortices in achiral spherical caps with the case of planar disks of a ferromagnet with an intrinsic DMI.

Taking into account that the Dzyaloshinskii constant $\mathcal{D}$ is determined by L, the vortex core profile should be dependent on the radius of the cap. This can be verified by comparing numerical solutions of Eq. (3) for the cases $\mathcal{D} \neq 0$ (spherical cap) and $\mathcal{D} = 0$ (disk). We performed micromagnetic simulations of the ground state for spherical caps with the thickness $h = 5$ nm and different inner radii and opening angles. To compare the size of the vortex core for different caps, we rely on the reduced coordinate along the cap meridian $s = L\vartheta/\ell$, see Fig. 4. We observe that the vortex core is slightly larger for the spherical cap with inner radius $L = 20$ nm and opening angle $\vartheta_0 = 175^\circ$ (blue diamonds in Fig. 4) than in the case of the cap with $L = 30$ nm and $\vartheta_0 = 115^\circ$ (green circles in Fig. 4). For comparison, the vortex core profile for a planar disk is displayed in Fig. 4 (red squares).

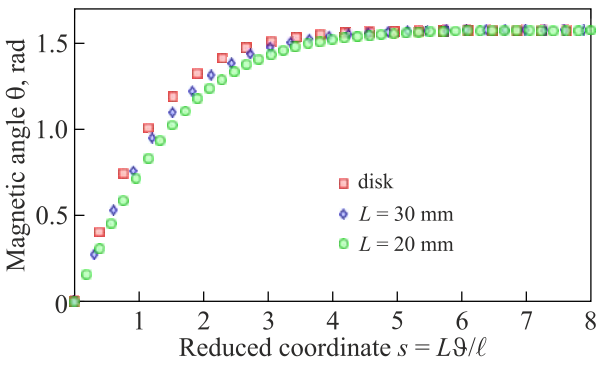

Fig. 4. (Color online) Vortex core profile for different curvature radii. Symbols correspond to the magnetic angle θ (describes the out-of-surface magnetization component) obtained from simulations for different curvature radii: green circles correspond to a spherical cap with the inner radius $L = 20$ nm, thickness $h = 5$ nm and opening angle $\vartheta_0 = 175°$; blue diamonds correspond to a spherical cap with the inner radius $L = 30$ nm, thickness $h = 5$ nm and opening angle $\vartheta_0 = 115°$; red squares correspond to planar disk with radius $L = 100$ nm and thickness $h = 5$ nm.

5. Conclusion

In conclusion, the geometric curvature of a spherical cap leads to the appearance of the effective coordinate-dependent anisotropy and DMI even for the case of intrinsically isotropic and achiral ferromagnets. Here, we derive and analyze the tilt of the azimuthal angle of magnetization for the vortex texture for the spherical cap geometry. The presence of curvature-induced DMI significantly modifies the properties of magnetic vortices. Namely, we observe a tilt of the magnetization at the edge of the cap, as well as a slight increase of the size of the magnetic vortex core. The obtained analytical results are verified using micromagnetic simulations of the models with full scale magnetostatics and easy-surface anisotropy.

The simulation results were obtained using the computing cluster of Taras Shevchenko National University of Kyiv [62]. This work is financed in part via the German Research Foundation (DFG) under Grants No. MA 5144/14-1, MA 5144/22-1, MA 5144/24-1, MC 9/22-1. V. P. K. acknowledges the Alexander von Humboldt Foundation for the support and Leibniz IFW Dresden for kind hospitality. M. I. S. and D. D. S. acknowledge HZDR, where a part of work was performed, for kind hospitality. M. I. S. acknowledges DAAD (Leonhard-Euler-Programm) for financial support. O. V. P. acknowledges a support within the program “Fuzzy continuous quantum measurements” of NAS of Ukraine (KPKVK 6541040).

1. S. S. P. Parkin, M. Hayashi, and L. Thomas, *Magnetic domain-wall racetrack memory*, *Sci.* **320**, 190 (2008).
2. R. Wiesendanger, *Nanoscale magnetic skyrmions in metallic films and multilayers: a new twist for spintronics*, *Nat. Rev. Mater.* **1**, 16044 (2016).
3. A. Fert, N. Reyren, and V. Cros, *Magnetic skyrmions: advances in physics and potential applications*, *Nat. Rev. Mater.* **2**, (2017).
4. D. Sander, S. O. Valenzuela, D. Makarov, C. H. Marrows, E. E. Fullerton, P. Fischer, J. McCord, P. Vavassori, S. Mangin, P. Pirro, B. Hillebrands, A. D. Kent, T. Jungwirth, O. Gutfleisch, C. G. Kim, and A. Berger, *J. Phys. D: Appl. Phys.* **50**, 363001 (2017).
5. E. Y. Vedmedenko, R. K. Kawakami, D. Sheka, P. Gambardella, A. Kirilyuk, A. Hirohata, C. Binek, O. A. Chubykalo-Fesenko, S. Sanvito, B. Kirby, J. Grollier, K. Everschor-Sitte, T. Kampfrath, C.-Y. You, and A. Berger, *J. Phys. D: Appl. Phys.* **53**, 453001 (2020).

6. C. Back, V. Cros, H. Ebert, K. Everschor-Sitte, A. Fert, M. Garst, T. Ma, S. Mankovsky, T. L. Monchesky, M. Mostovoy, N. Nagaosa, S. S. P. Parkin, C. Pfleiderer, N. Reyren, A. Rosch, Y. Taguchi, Y. Tokura, K. von Bergmann, and J. Zang, *J. Phys. D: Appl. Phys.* **53**, 363001 (2020).
7. E. Feldtkeller and H. Thomas, *Z. Phys. B: Condens. Matter* **4**, 8 (1965).
8. A. M. Kosevich, V. P. Voronov, and I. V. Manzhos, *Nonlinear cooperative excitations in easy-plane magnet*, *Sov. Phys. JETP* **57**, 148 (1983).
9. R. P. Cowburn, *Property variation with shape in magnetic nanoelements*, *J. Phys. D: Appl. Phys.* **33**, R1 (2000).
10. K. Y. Guslienko, *Magnetic vortex state stability, reversal and dynamics in restricted geometries*, *J. Nanosci. Nanotechnol.* **8**, 2745 (2008).
11. A. Hubert and R. Schäfer, *Magnetic Domains: The Analysis of Magnetic Microstructures*, Springer-Berlin-Heidelberg, Berlin (2009).
12. A. Fernández-Pacheco, R. Streubel, O. Fruchart, R. Hertel, P. Fischer, and R. P. Cowburn, *Three-dimensional nanomagnetism*, *Nat. Commun*. **8**, 15756 (2017).
13. M. Kläui, C. A. F. Vaz, L. Lopez-Diaz, and J. A. C. Bland, *Vortex formation in narrow ferromagnetic rings*, *J. Phys.: Condens. Matter* **15**, R985 (2003).
14. V. P. Kravchuk, D. D. Sheka, and Y. B. Gaididei, *Equilibrium magnetisation structures in ferromagnetic nanorings*, *J. Magn. Magn. Mater.* **310**, 116 (2007).
15. D. D. Sheka, V. P. Kravchuk, M. I. Sloika, and Y. Gaididei, *Equilibrium states of soft magnetic hemispherical shell*, *SPIN* **3**, 1340003 (2013).
16. R. Streubel, D. Makarov, F. Kronast, V. Kravchuk, M. Albrecht, and O. G. Schmidt, *Magnetic vortices on closely packed spherically curved surfaces*, *Phys. Rev. B* **85**, 174429 (2012).
17. D. Mitin, D. Nissen, P. Schädlich, S. S. P. K. Arekapudi, and M. Albrecht, *Single vortex core recording in a magnetic vortex lattice*, *J. Appl. Phys.* **115**, 063906 (2014).
18. D. Nissen, D. Mitin, O. Klein, S. S. P. K. Arekapudi, S. Thomas, M.-Y. Im, P. Fischer, and M. Albrecht, *Magnetic coupling of vortices in a two-dimensional lattice*, *Nanotechnology* **26**, 465706 (2015).
19. R. Streubel, F. Kronast, C. F. Reiche, T. Mühl, A. U. B. Wolter, O. G. Schmidt, and D. Makarov, *Vortex circulation and polarity patterns in closely packed cap arrays*, *Appl. Phys. Lett*. **108**, 042407 (2016).
20. V. P. Kravchuk, D. D. Sheka, and Y. Gaididei, *Out-of-surface vortices in spherical shells*, *Phys. Rev. B* **85**, 144433 (2012).
21. M. I. Sloika, D. D. Sheka, V. P. Kravchuk, O. V. Pylypovskyi, and Y. Gaididei, *Geometry induced phase transitions in magnetic spherical shell*, *J. Magn. Magn. Mater.* **443**, 404 (2017).
22. V. L. Carvalho-Santos, W. A. Moura-Melo, and A. R. Pereira, *Miniaturization of vortex-comprising system using ferromagnetic nanotori*, *J. Appl. Phys.* **108**, 094310 (2010).
23. S. Vojkovic, A. S. Nunez, D. Altbir, and V. L. Carvalho-Santos, *Magnetization ground state and reversal modes of magnetic nanotori*, *J. Appl. Phys*. **120**, 033901 (2016).
24. V. Carvalho-Santos, F. Apolonio, and N. Oliveira-Neto, *On geometry-dependent vortex stability and topological spin excitations on curved surfaces with cylindrical symmetry*, *Phys. Lett. A* **377**, 1308 (2013).
25. D. Mancilla-Almonacid, M. Castro, J. Fonseca, D. Altbir, S. Allende, and V. Carvalho-Santos, *Magnetic ground states for bent nanotubes*, *J. Magn. Magn. Mater.* **507**, 166754 (2020).
26. D. Makarov, O. M. Volkov, A. Kákay, O. V. Pylypovskyi, B. Budinská, and O. V. Dobrovolskiy, *New dimension in magnetism and superconductivity: 3D and curvilinear nanoarchitectures*, *Adv. Mater*. **34**, 2101758 (2022).
27. D. D. Sheka, O. V. Pylypovskyi, O. M. Volkov, K. V. Yershov, V. P. Kravchuk, and D. Makarov, *Fundamentals of curvilinear ferromagnetism: Statics and dynamics of geometrically curved wires and narrow ribbons*, *Small* **18**, 2105219 (2022).
28. P. Landeros and A. S. Núñez, *Domain wall motion on magnetic nanotubes*, *J. App. Phys*. **108**, 033917 (2010).
29. V. P. Kravchuk, U. K. Rößler, O. M. Volkov, D. D. Sheka, J. van den Brink, D. Makarov, H. Fuchs, H. Fangohr, and Y. Gaididei, *Topologically stable magnetization states on a spherical shell: Curvature-stabilized skyrmions*, *Phys. Rev. B* **94**, 144402 (2016).
30. A. Teixeira, S. Castillo-Sepúlveda, S. Vojkovic, J. Fonseca, D. Altbir, Á. Núñez, and V. Carvalho-Santos, *Analysis on the stability of in-surface magnetic configurations in toroidal nanoshells*, *J. Magn. Magn. Mater.* **478**, 253 (2019).
31. M. Staňo and O. Fruchart, *Magnetic nanowires and nanotubes*, in *Handbook of Magnetic Materials*, Elsevier, (2018) pp. 155–267.
32. S. Castillo-Sepúlveda, R. Cacilhas, V. L. Carvalho-Santos, R. M. Corona, and D. Altbir, *Magnetic hopfions in toroidal nanostructures driven by an Oersted magnetic field*, *Phys. Rev. B* **104**, (2021).
33. R. Hertel, *Curvature–induced magnetochirality*, *SPIN* **3**, 1340009 (2013).
34. R. Streubel, P. Fischer, F. Kronast, V. P. Kravchuk, D. D. Sheka, Y. Gaididei, O. G. Schmidt, and D. Makarov, *Magnetism in curved geometries* (Topical Review), *J. Phys. D: Appl. Phys.* **49**, 363001 (2016).
35. C. Dietrich, R. Hertel, M. Huber, D. Weiss, R. Schäfer, and J. Zweck, *Influence of perpendicular magnetic fields on the domain structure of permalloy microstructures grown on thin membranes*, *Phys. Rev. B* **77**, 174427 (2008).
36. M. Yan, C. Andreas, A. Kákay, F. García-Sánchez, and R. Hertel, *Fast domain wall dynamics in magnetic nanotubes: Suppression of Walker breakdown and Cherenkov-like spin wave emission*, *Appl. Phys. Lett*. **99**, 122505 (2011).
37. M. Yan, C. Andreas, A. Kákay, F. Garcia-Sanchez, and R. Hertel, *Chiral symmetry breaking and pair-creation mediated Walker breakdown in magnetic nanotubes*, *Appl. Phys. Lett*. **100**, 252401 (2012).

38. J. A. Otálora, M. Yan, H. Schultheiss, R. Hertel, and A. Kákay, *Curvature-induced asymmetric spin-wave dispersion*, *Phys. Rev. Lett*. **117**, 227203 (2016).
39. D. D. Sheka, *A perspective on curvilinear magnetism*, *Appl. Phys. Lett*. **118**, 230502 (2021).
40. V. P. Kravchuk, D. D. Sheka, R. Streubel, D. Makarov, O. G. Schmidt, and Y. Gaididei, *Out-of-surface vortices in spherical shells*, *Phys. Rev. B* **85**, 144433 (2012).
41. M. I. Sloika, V. P. Kravchuk, D. D. Sheka, and Y. Gaididei, *Curvature induced chirality symmetry breaking in vortex core switching phenomena*, *Appl. Phys. Lett*. **104**, 252403 (2014).
42. Y. Gaididei, V. P. Kravchuk, and D. D. Sheka, *Curvature effects in thin magnetic shells*, *Phys. Rev. Lett*. **112**, 257203 (2014).
43. D. D. Sheka, V. P. Kravchuk, and Y. Gaididei, *Curvature effects in statics and dynamics of low dimensional magnets*, *J. Phys. A:* **48**, 125202 (2015).
44. D. D. Sheka, O. V. Pylypovskyi, P. Landeros, Y. Gaididei, A. Kákay, and D. Makarov, *Nonlocal chiral symmetry breaking in curvilinear magnetic shells*, *Commun. Phys*. **3**, 128 (2020).
45. I. E. Dzialoshinskii, *Thermodynamic theory of "weak" ferromagnetism in antiferromagnetic substances*, *Sov. Phys. JETP* **5**, 1259 (1957).
46. T. Moriya, *Anisotropic superexchange interaction and weak ferromagnetism*, *Phys. Rev*. **120**, 91 (1960).
47. O. V. Pylypovskyi, V. P. Kravchuk, D. D. Sheka, D. Makarov, O. G. Schmidt, and Y. Gaididei, *Coupling of chiralities in spin and physical spaces: The Möbius ring as a case study*, *Phys. Rev. Lett.* **114**, 197204 (2015).
48. V. P. Kravchuk, D. D. Sheka, A. Kákay, O. M. Volkov, U. K. Rößler, J. van den Brink, D. Makarov, and Y. Gaididei, *Multiplet of skyrmion states on a curvilinear defect*: *Reconfigurable skyrmion lattices*, *Phys. Rev. Lett.* **120**, 067201 (2018).
49. O. V. Pylypovskyi, D. Makarov, V. P. Kravchuk, Y. Gaididei, A. Saxena, and D. D. Sheka, *Chiral skyrmion and skyrmionium states engineered by the gradient of curvature*, *Phys. Rev. Appl*. **10**, 064057 (2018).
50. A. B. Butenko, A. A. Leonov, A. N. Bogdanov, and U. K. Rößler, *Theory of vortex states in magnetic nanodisks with induced Dzyaloshinskii–Moriya interactions*, *Phys. Rev. B* **80**, 134410 (2009).
51. G. Gioia and R. D. James, *Micromagnetics of very thin films*, *Proc. R. Soc A* **453**, 213 (1997).
52. G. Carbou, *Thin layers in micromagnetism*, *Math. Models Methods Appl. Sci*. (M3AS) **11**, 1529 (2001).
53. A. Desimone, R. V. Kohn, S. Müller, and F. Otto, *A reduced theory for thin-film micromagnetics*, *Comm. Pure Appl. Math.* **55**, 1408 (2002)
54. R. V. Kohn and V. V. Slastikov, *Another thin-film limit of micromagnetics*, *Arch. Ration. Mech. Anal.* **178**, 227 (2005).
55. V. Slastikov, *Micromagnetism of thin shells*, *Math. Models Methods Appl. Sci*. **15**, 1469 (2005).
56. G. Di Fratta, *Micromagnetics of curved thin films*, *Z. Angew. Math. Phys*. **71**, 111 (2020).
57. R. Streubel, V. P. Kravchuk, D. D. Sheka, D. Makarov, F. Kronast, O. G. Schmidt, and Y. Gaididei, *Equilibrium magnetic states in individual hemispherical permalloy caps*, *Appl. Phys. Lett.* **101**, 132419 (2012).
58. A. B. Butenko, A. A. Leonov, A. N. Bogdanov, and U. K. Rößler, *Influence of the Dzyaloshinskii-Moriya interaction on vortex states in magnetic nanodisks*, *J. Physics: Conf. Ser*. **200**, 042012 (2010).
59. M.-Y. Im, P. Fischer, K. Yamada, T. Sato, Shinya Kasai, Y. Nakatani, and T. Ono, *Symmetry breaking in the formation of magnetic vortex states in a permalloy nanodisk*, *Nat. Commun*. **3**, 983 (2012).
60. MAGPAR finite element micromagnetics package, developed by Werner Scholz.
61. W. Scholz, J. Fidler, T. Schrefl, D. Suess, R. Dittrich, H. Forster, and V. Tsiantos, *Scalable parallel micromagnetic solvers for magnetic nanostructures*, *Comput. Mater. Sci*. **28**, 366 (2003), Proceedings of the Symposium on Software Development for Process and Materials Design.
62. High–performance computing cluster of Taras Shevchenko National University of Kyiv, http://cluster.univ.kiev.ua/eng/

Вплив індукованої кривиною взаємодії Дзялошинського–Морія на магнітний вихор у сферичних шапках

Mykola I. Sloika, Yuri Gaididei,
Volodymyr P. Kravchuk, Oleksandr V. Pylypovskyi,
Denys Makarov, Denis D. Sheka

Геометрична кривина нанорозмірних магнітних оболонок спричиняє анізотропію та взаємодію Дзялошинського–Морія (ВДМ). Представлено рівняння для опису профілю стану магнітного вихору у сферичній шапці. Продемонстровано, що азимутальна складова намагніченості набуває кінцевого нахилу на краю шапки, що призводить до збільшення магнітної поверхневої енергії, на відміну від випадку замкненої сферичної оболонки, де симетрія текстури не уможливлює будь-якого нахилу намагніченості на екваторі сфери. Проаналізовано розмір ядра вихору у сферичній шапці та показано, що наявність ВДМ, яка індукована кривиною, призводить до збільшення розміру ядра незалежно від добутку циркуляції та полярності вихору. Це відрізняється від випадку плоских дисків із власною ВДМ, де переважний напрямок циркуляції, а також зменшення або збільшення розміру вихрового ядра визначається знаком добутку циркуляції та полярністю по відношенню до знаку константи власної ВДМ.

Ключові слова: взаємодія Дзялошинського–Морія, сферична шапка, магнітно-вихровий стан.